Published for SISSA by Springer

Received: *March 29, 2024*
Revised: *May 3, 2024*
Accepted: *May 9, 2024*
Published: *May 31, 2024*

Measurement of absolute branching fractions of D_s^+ hadronic decays

The BESIII collaboration

E-mail: besiii-publications@ihep.ac.cn

Abstract: Using e^+e^- collision data collected at the BESIII detector at center-of-mass energies between 4.128 and 4.226 GeV, corresponding to an integrated luminosity of $7.33\,\mathrm{fb}^{-1}$, we determine the absolute branching fractions of fifteen hadronic D_s^+ decays with a double-tag technique. In particular, we make precise measurements of the branching fractions $\mathcal{B}(D_s^+ \to K^+K^-\pi^+) = (5.49 \pm 0.04 \pm 0.07)\%$, $\mathcal{B}(D_s^+ \to K_S^0 K^+) = (1.50 \pm 0.01 \pm 0.01)\%$ and $\mathcal{B}(D_s^+ \to K^+K^-\pi^+\pi^0) = (5.50 \pm 0.05 \pm 0.11)\%$, where the first uncertainties are statistical and the second ones are systematic. The CP asymmetries in these decays are also measured and all are found to be compatible with zero.

Keywords: Branching fraction, Charm Physics, CP Violation, e^+-e^- Experiments

ArXiv ePrint: 2403.19256

https://doi.org/10.1007/JHEP05(2024)335

JHEP05(2024)335

Contents

1 Introduction

Hadronic D_s^+ decays play an important role in both charm and beauty physics. Precise measurements of the absolute branching fractions (BF) of hadronic D_s^+ decays provide useful information to understand the underlying decay mechanism and help improve theoretical models [1–8]. The $D_s^+ \to K^+K^-\pi^+$, $D_s^+ \to K_S^0\pi^+$, and $D_s^+ \to K^+K^-\pi^+\pi^0$ decays are not only used as the reference modes for measurements of relative BFs of D_s^+ decays, but also used to measure the modulus of the Cabibbo-Kobayashi-Maskawa matrix element $|V_{cb}|$ in decays $B_s^0 \to D_s^- X$ [9]. Furthermore, searching for *CP* asymmetries in hadronic $D_s^\pm$ decays allows a more comprehensive understanding of *CP* violation in the charm sector. Therefore, precision measurements of the absolute BFs of hadronic D_s^+ are an important component of the experimental and theoretical heavy-flavor physics program.

In this paper, we perform the measurements of the absolute BFs of fifteen D_s^+ decays: $K_S^0K^+$, $K^+K^-\pi^+$, $K_S^0K^+\pi^0$, $K_S^0K_S^0\pi^+$, $K^+K^-\pi^+\pi^0$, $K_S^0K^+\pi^+\pi^-$, $K_S^0K^-\pi^+\pi^+$, $\pi^+\pi^+\pi^-$, $\pi^+\eta$, $\pi^+\pi^0\eta$, $\pi^+\pi^+\pi^-\eta$, $\pi^+\eta'$, $\pi^+\pi^0\eta'$, $K_S^0\pi^+\pi^0$, $K^+\pi^+\pi^-$, based on a sample of e^+e^- annihilation data corresponding to an integrated luminosity of 7.33 fb^{-1} taken at the center-of-mass energies in the interval $\sqrt{s} = 4.128$–4.226 GeV with the BESIII detector [10]. Thirteen of these decay modes have been previously measured by the CLEO-c collaboration [11]. Moreover, *CP* asymmetries for these decays are measured in this paper. Throughout this paper, charge-conjugated processes are implied except in *CP* asymmetry measurements.

2 Measurement technique

The double-tag (DT) method [12] is employed to obtain clean signal samples of $e^+e^- \to D_s^{*\pm}D_s^{\mp} \to (\gamma,\pi^0)D_s^+D_s^-$ in the following analyses. The transition photon or π^0 is not reconstructed. In this analysis, a single-tag (ST) candidate requires only one of the $D_s^{\pm}$ mesons to be reconstructed via a hadronic decay, and a DT candidate has both D_s^+ and D_s^- mesons reconstructed via hadronic decays. Considering two ST modes, $D_s^+ \to i$ and $D_s^- \to \bar{j}$, and one DT mode $D_s^+ \to i$, $D_s^- \to \bar{j}$, the BF for the i and $\bar{j}$ decays are $\mathcal{B}_i$ and $\mathcal{B}_{\bar{j}}$. We assume CP violation is negligible while determining the BF ($\mathcal{B}_j = \mathcal{B}_{\bar{j}}$), then we have:

$$\begin{aligned} Y_i &= N^{D_s^+D_s^-}\mathcal{B}_i\epsilon_i\,, \\ Y_{\bar{j}} &= N^{D_s^+D_s^-}\mathcal{B}_{\bar{j}}\epsilon_{\bar{j}}\,, \\ Y_{i\bar{j}} &= N^{D_s^+D_s^-}\mathcal{B}_i\mathcal{B}_{\bar{j}}\epsilon_{i\bar{j}}\,, \end{aligned} \tag{2.1}$$

where ϵ_i and $\epsilon_{\bar{j}}$ are the ST efficiencies, $\epsilon_{i\bar{j}}$ is the DT efficiency, Y_i and $Y_{\bar{j}}$ are the expected ST yields, $Y_{i\bar{j}}$ is the expected DT yield, and $N^{D_s^+D_s^-}$ is the number of $D_s^+D_s^-$ pairs.

For ST and DT yields, we calculate the expected yields based on eq. (2.1) using B_i, $B_{\bar{j}}$ and $N^{D_s^+D_s^-}$, and perform a maximum likelihood fit to the obtained ST and DT yields. Through the fit, we obtain the results of the parameters, considering both statistical and systematic uncertainties.

We constrain $\mathcal{B}_i$ to be the same for different final states involving η (η') in the intermediate state, taking into account different detection efficiencies and BFs of the η (η') meson.

We analyze fifteen decay modes (nineteen final states) and seven data sample groups (see table 1), leading to a total of 266 ($19 \times 2 \times 7$) ST yields, 2527 ($19 \times 19 \times 7$) DT yields, fifteen BFs and seven $N^{D_s^+D_s^-}$ values.

We derive the CP asymmetry for each decay mode by:

$$\mathcal{A}_{CP,i} = \frac{N_i/\epsilon_i - N_{\bar{i}}/\epsilon_{\bar{i}}}{N_i/\epsilon_i + N_{\bar{i}}/\epsilon_{\bar{i}}}, \tag{2.2}$$

where N_i ($N_{\bar{i}}$) is the obtained yield for ST mode i ($\bar{i}$).

3 Detector and data sets

The BESIII detector [10] records symmetric e^+e^- collisions provided by the BEPCII storage ring [13] in the center-of-mass energy range from 2.0 to 4.95 GeV, with a peak luminosity of $1 \times 10^{33}\,\mathrm{cm^{-2}\,s^{-1}}$ achieved at $\sqrt{s} = 3.77$ GeV. The cylindrical core of the BESIII detector covers 93% of the full solid angle and consists of a helium-based multilayer drift chamber (MDC), a plastic scintillator time-of-flight system (TOF), and a CsI(Tl) electromagnetic calorimeter (EMC), which are all enclosed in a superconducting solenoidal magnet providing a 1.0 T magnetic field [14]. The solenoid is supported by an octagonal flux-return yoke with resistive plate counter muon identification modules interleaved with steel. The charged-particle momentum resolution at 1 GeV/c is 0.5%, and the dE/dx resolution is 6% for electrons from Bhabha scattering. The EMC measures photon energies with a resolution of 2.5% (5%) at 1 GeV in the barrel (end cap) region. The time resolution in the TOF barrel region is

JHEP05(2024)335

$\sqrt{s}$ (GeV)	$\mathcal{L}_{\rm int}$ (pb^{-1})	$M_{\rm rec}$ (GeV/c^2)
4.128	401.5	$[2.060, 2.150]$
4.157	408.7	$[2.054, 2.170]$
4.178	$3189.0 \pm 0.2 \pm 31.9$	$[2.050, 2.180]$
4.189	$570.0 \pm 0.1 \pm 2.2$	$[2048, 2.190]$
4.199	$526.0 \pm 0.1 \pm 2.1$	$[2.046, 2.200]$
4.209	$572.1 \pm 0.1 \pm 1.8$	$[2.044, 2.210]$
4.219	$569.2 \pm 0.1 \pm 1.8$	$[2.042, 2.220]$
4.226	$1100.9 \pm 0.1 \pm 7.0$	$[2.040, 2.220]$

Table 1. The integrated luminosities ($\mathcal{L}_{\rm int}$) and the requirements on $M_{\rm rec}$ for various center-of-mass energies [20, 21]. The first and second uncertainties are statistical and systematic, respectively. The definition of $M_{\rm rec}$ is given in eq. (4.1). The integrated luminosities for data samples of $\sqrt{s} = 4.128$ GeV and $\sqrt{s} = 4.157$ GeV are estimated by using online monitoring information.

68 ps, while that in the end cap region is 110 ps. The end cap TOF system was upgraded in 2015 using multigap resistive plate chamber technology, providing a time resolution of 60 ps [15–17]. About 84% of the data used in this paper benefits from this upgrade.

Data samples corresponding to a total integrated luminosity of 7.33 fb^{-1} are used in this paper. The integrated luminosities for the individual center-of-mass energies [18] are given in table 1. Data samples of $\sqrt{s} = 4.128$ GeV and $\sqrt{s} = 4.157$ GeV are merged into one group due to their low statistics. Since the cross section of $e^+e^- \to D_s^{*\pm}D_s^{\mp}$ production in e^+e^- annihilation is about twenty times larger than the one of $e^+e^- \to D_s^+D_s^-$ [19] in this energy region, the signal events discussed in this paper are selected from the process $e^+e^- \to D_s^{*\pm}D_s^{\mp}$.

To determine the detection efficiencies and estimate backgrounds, we produce and analyze GEANT4-based [22] Monte Carlo (MC) simulation samples for all data sets listed in table 1, with sizes that are 40 times the integrated luminosity of data. The MC samples are produced using known decay rates [23] and correct angular distributions by two event generators, EVTGEN [24] for charm ($D_s^{*\pm}$, $D_s^{\pm}$, $D^{*0(\pm)}$, and $D^{0(\pm)}$) and charmonium decays and KKMC [25] for continuum processes. The samples consist of $e^+e^- \to D\bar{D}$, D^*D, D^*D^*, D_sD_s, $D_s^*D_s$, $D_s^*D_s^*$, $DD^*\pi$, $DD\pi$, $q\bar{q}\,(q = u, d, s)$, $\gamma J/\psi$, $\gamma\,\psi(3686)$, and $\tau^+\tau^-$. For the fifteen D_s^+ signal processes, twelve multi-body processes are generated based on amplitude models [26–36],[1] while the three two-body processes are modeled with a uniform phase-space distribution. Charmonium decays that are not accounted for by exclusive measurements are simulated by LUNDCHARM [37]. All MC simulations include the effects of initial-state radiation (ISR) and final-state radiation (FSR). We simulate ISR with ConExc [38] for $e^+e^- \to c\bar{c}$ events within the framework of EVTGEN, and with KKMC for non-charm continuum processes. The simulation models the beam energy spread in the e^+e^- annihilations with the generator KKMC. FSR from charged final state particles is incorporated using PHOTOS [39].

[1]The amplitude model for the $K_S^0K^+\pi^+\pi^-$ mode is taken from an unpublished BESIII internal results, which are on going.

4 Event selection

The $D_s^\pm$ candidates are constructed from combinations of $\pi^\pm$, $K^\pm$, K_S^0, η, η', $\rho(770)^0$, and γ candidates in nineteen final states. The $D_s^+ \to \pi^+\eta$ decay is reconstructed via two distinct final states, $D_s^+ \to \pi^+\eta_{\gamma\gamma}$ and $D_s^+ \to \pi^+\eta_{\pi^+\pi^-\pi^0}$. The $D_s^+ \to \pi^+\eta'$ is reconstructed in three final states $D_s^+ \to \pi^+\eta'_{\pi^+\pi^-\eta_{\gamma\gamma}}$, $D_s^+ \to \pi^+\eta'_{\pi^+\pi^-\eta_{\pi^+\pi^-\pi^0}}$, and $D_s^+ \to \pi^+\eta'_{\gamma\rho}$. The $D_s^+ \to \pi^+\pi^0\eta'$ is reconstructed in two final states which are $D_s^+ \to \pi^+\pi^0\eta'_{\pi^+\pi^-\eta_{\gamma\gamma}}$, and $D_s^+ \to \pi^+\pi^0\eta'_{\gamma\rho}$. Here, the subscripts on $\eta_{\gamma\gamma}$, $\eta_{\pi^+\pi^-\pi^0}$, $\eta'_{\pi^+\pi^-\eta}$, and $\eta'_{\gamma\rho}$ indicate the reconstructed decay modes $\eta \to \gamma\gamma$, $\eta \to \pi^+\pi^-\pi^0$, $\eta' \to \pi^+\pi^-\eta$ and $\eta' \to \gamma\rho$, where ρ denotes $\rho(770)^0$.

All charged tracks detected in the MDC are required to be within a polar angle (θ) range of $|\cos\theta| < 0.93$, where θ is defined with respect to the z-axis, which is the symmetry axis of the MDC. For charged tracks not originating from K_S^0 decays, the distance of closest approach to the interaction point (IP) must be less than 10 cm along the z-axis, $|V_z|$, and less than 1 cm in the transverse plane, $|V_{xy}|$. Particle identification (PID) for charged tracks combines measurements of the $\mathrm{d}E/\mathrm{d}x$ in the MDC and the flight time in the TOF to form likelihoods $\mathcal{L}\ (h)$ $(h = K, \pi)$ for each hadron h hypothesis. The charged kaons and pions are identified by requiring $\mathcal{L}\ (K) > \mathcal{L}\ (\pi)$ and $\mathcal{L}\ (\pi) > \mathcal{L}\ (K)$, respectively.

The K_S^0 candidates are reconstructed from pairs of oppositely charged tracks satisfying $|V_z| < 20$ cm. The two charged tracks are assigned as $\pi^+\pi^-$ without imposing the above PID criteria. The quality of the vertex fits is ensured by a requirement of $\chi^2 < 100$. The invariant mass of the $\pi^+\pi^-$ pair is required to be within $[0.487, 0.511]$ GeV$/c^2$. For the $D_s^+ \to K_S^0K_S^0\pi^+$ and $D_s^+ \to K_S^0\pi^+\pi^0$ modes, to avoid the peaking background from $D_s^+ \to \pi^+\pi^+\pi^+\pi^-\pi^-$ and $D_s^+ \to \pi^+\pi^+\pi^-\pi^0$ modes, the decay length from the IP of the K_S^0 candidate is required to be greater than twice the resolution.

Photon candidates are identified using showers in the EMC. The deposited energy of each shower must be more than 25 MeV in the barrel region ($|\cos\theta| < 0.80$) and more than 50 MeV in the end cap region ($0.86 < |\cos\theta| < 0.92$). To exclude showers that originate from charged tracks, the angle subtended by the EMC shower and the position of the closest charged track at the EMC must be greater than 10 degrees as measured from the IP. To suppress electronic noise and showers unrelated to the event, the difference between the EMC time and the event start time is required to be within [0, 700] ns.

The π^0 and $\eta_{\gamma\gamma}$ candidates are reconstructed from photon pairs with invariant masses in the ranges $[0.115, 0.150]$ GeV$/c^2$ and $[0.490, 0.580]$ GeV$/c^2$, respectively. We require that at least one photon comes from the barrel region of the EMC to improve their invariant mass resolutions. A kinematic fit constraining the invariant mass of the selected photon pair to the known π^0 or η mass [23] is performed, and the χ^2 of the kinematic fit is required to be less than 30. The $\eta_{\pi^+\pi^-\pi^0}$ candidates are formed from $\pi^+\pi^-\pi^0$ combinations with an invariant mass in the range $[0.530, 0.560]$ GeV$/c^2$.

For the η' candidates formed from $\pi^+\pi^-\eta$ and $\gamma\rho(770)^0$ combinations, we require invariant masses to be within the ranges $[0.943, 0.973]$ GeV$/c^2$ and $[0.946, 0.970]$ GeV$/c^2$, respectively. Furthermore, the $\rho(770)^0$ candidates are formed from $\pi^+\pi^-$ combinations with an invariant mass within the range $[0.570, 0.970]$ GeV$/c^2$.

For the $D_s^+ \to K^+\pi^+\pi^-$ mode, we require the $\pi^+\pi^-$ invariant mass to be outside of the range $[0.487, 0.511]$ GeV$/c^2$ to exclude the $K_S^0 \to \pi^+\pi^-$ contamination from the process

$D_s^+ \to K_S^0 K^+$. Similarly, for the $D_s^+ \to \pi^+\pi^+\pi^-\eta$ mode, we require the $\pi^+\pi^-\eta$ invariant mass to be outside of the range $[0.943, 0.973]\,\mathrm{GeV}/c^2$ to exclude the $\eta' \to \pi^+\pi^-\eta$ contribution from the process $D_s^+ \to \pi^+\eta'$.

The invariant masses of $D_s^\pm$ candidates ($M_{D_s^\pm}$) are required to be in the range of $[1.88, 2.06]\,\mathrm{GeV}/c^2$. The recoil mass $M_{\rm rec}$ is defined as

$$M_{\rm rec}^2 c^4 = \left(\sqrt{s} - \sqrt{|\vec{p}_{D_s^+}|^2 c^2 + m_{D_s^+}^2 c^4}\right)^2 - \left|\vec{p}_{D_s^+}\right|^2 c^2\,, \tag{4.1}$$

where $\vec{p}_{D_s^+}$ is the three-momentum of the D_s^+ candidate in the e^+e^- center-of-mass frame and $m_{D_s^+}$ is the known D_s^+ mass [23]. We use two different requirements on $M_{\rm rec}$: a tighter selection, within the interval of $[2.10, 2.13]\,\mathrm{GeV}/c^2$, for $D_s^+ \to \pi^+\pi^+\pi^-\eta$, $D_s^+ \to \pi^+\pi^0\eta'_{\gamma\rho}$, and $D_s^+ \to K_S^0\pi^+\pi^0$ final states for all energy points to reduce background, and the looser intervals given in table 1 for the remaining final states. If there are multiple ST candidates, the candidate with the $M_{\rm rec}$ closest to the known D_s^{*+} mass [23] is kept.

The DT $D_s^\pm$ candidates are required to pass the same selections as those for ST candidates, and we require one of the two $D_s^\pm$ candidates to satisfy $M_{\rm rec} > 2.10\,\mathrm{GeV}/c^2$. If there are multiple combinations in an event, the combination with the average $D_s^\pm$ candidate invariant mass ($\overline{m} = (M_{D_s^+} + M_{D_s^-})/2$) closest to the known $D_s^\pm$ mass [23] is retained. About 19.7% (20.1%) of events in data (simulated samples) contain multiple DT candidates, and the distributions of the multiplicity of DT candidate show good consistency between data and simulated samples. This requirement retains more than 97.7% of DT signal candidates.

5 Single-tag and double-tag yields

The ST yields are determined from fits to the $M_{D_s^\pm}$ distributions. As an example, the fits to the $M_{D_s^+}$ and $M_{D_s^-}$ distributions of the selected ST candidates from the data sample at $\sqrt{s} = 4.178\,\mathrm{GeV}$ are shown in figure 1 and figure 2, respectively. We use the MC-simulated shape convolved with a Gaussian function to describe the signal. The background is described by a second-order polynomial. The MC-simulated shapes of the final states $D^+ \to K_S^0\pi^+$ and $D_s^+ \to \pi^+\pi^+\pi^-\eta_{\gamma\gamma}$ are included as peaking background components in the fits for the final states $D_s^+ \to K_S^0 K^+$ and $D_s^+ \to \pi^+\eta'_{\pi^+\pi^-\eta_{\gamma\gamma}}$, respectively. The various ST yields in data at $\sqrt{s} = 4.178\,\mathrm{GeV}$ are summarized in table 2.

Since each ST final state may receive crossfeed background from other ST signal final states, we create an efficiency-correction matrix, $\mathbf{C}^{\rm ST}$, to describe simultaneously the detection efficiencies (diagonal elements) and the crossfeed probabilities (off-diagonal elements) [40]. The elements $\mathbf{C}^{\rm ST}_{ij}$ are defined to be the probabilities that an event of signal mode j is reconstructed and counted in the yield for mode i, as determined using MC samples.

The DT yields are determined by counting events in a signal and two sideband regions in the plane of $M_{D_s^+}$ versus $M_{D_s^-}$. This provides a unified method that works well, considering the low statistics of some DT final states. Figure 3 shows the $M_{D_s^+}$ versus $M_{D_s^-}$ distribution of all DT candidates in data, as well as the signal and the sideband regions. The signal region requires that the average invariant mass satisfy $|\overline{m} - m_{D_s^+}| < 15\,\mathrm{MeV}/c^2$ while the invariant mass difference $\Delta m = M_{D_s^+} - M_{D_s^-}$ satisfies $|\Delta m| < 30\,\mathrm{MeV}/c^2$. We define a sideband region with the same $\overline{m}$ requirement but with $80 < |\Delta m| < 140\,\mathrm{MeV}/c^2$. The

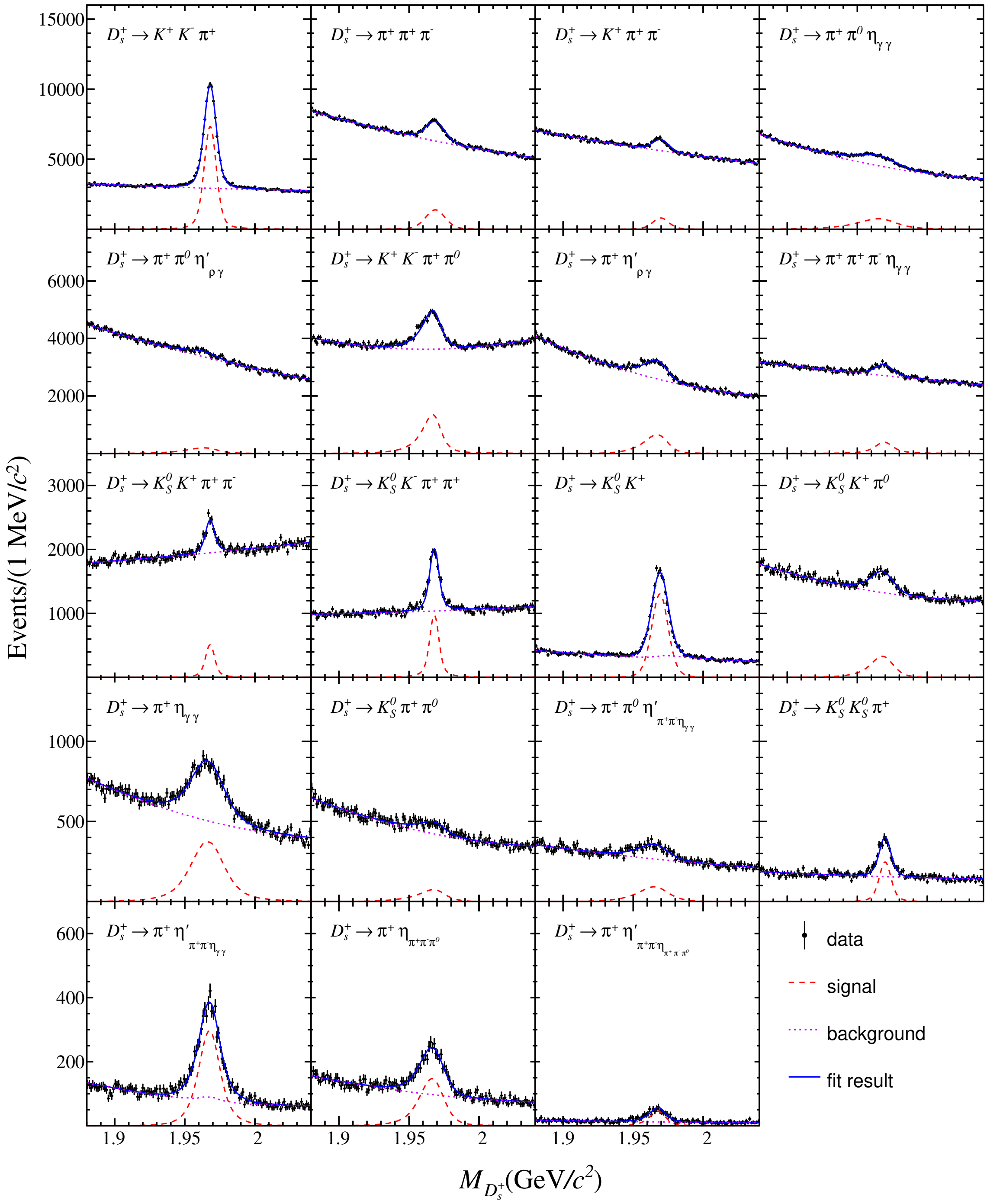

Figure 1. Fits to the $M_{D_s^+}$ distributions of the ST candidates from the data sample at $\sqrt{s} = 4.178$ GeV. The points with error bars are data, the blue solid curves are the fit results, the pink dotted curves are the fitted background shapes, and the red dashed curves are the signals.

JHEP05(2024)335

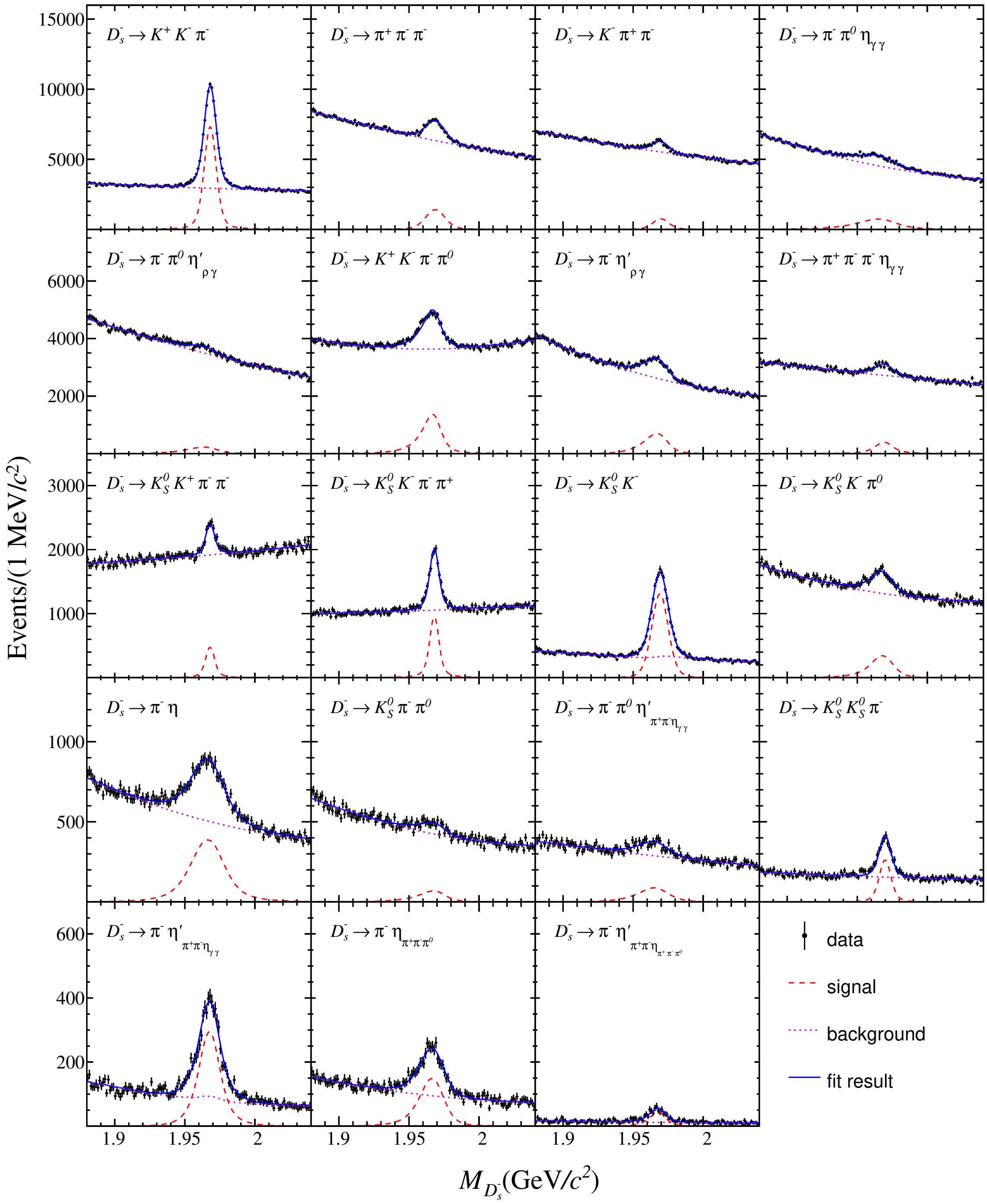

Figure 2. Fits to the $M_{D_s^-}$ distributions of the ST candidates from the data sample at $\sqrt{s} = 4.178\,\text{GeV}$. The points with error bars are data, the blue solid curves are the fit results, the pink dotted curves are the fitted background shapes, and the red dashed curves are the signals.

Final state	Yield	Final state	Yield
$D_s^+ \to K_S^0 K^+$	16668 ± 166	$D_s^- \to K_S^0 K^-$	16739 ± 166
$D_s^+ \to K^+ K^- \pi^+$	73252 ± 379	$D_s^- \to K^+ K^- \pi^-$	73048 ± 380
$D_s^+ \to K_S^0 K^+ \pi^0$	6375 ± 249	$D_s^- \to K_S^0 K^- \pi^0$	6616 ± 249
$D_s^+ \to K_S^0 K_S^0 \pi^+$	2546 ± 79	$D_s^- \to K_S^0 K_S^0 \pi^-$	2686 ± 80
$D_s^+ \to K^+ K^- \pi^+ \pi^0$	24033 ± 425	$D_s^- \to K^+ K^- \pi^- \pi^0$	24295 ± 426
$D_s^+ \to K_S^0 K^+ \pi^+ \pi^-$	4944 ± 217	$D_s^- \to K_S^0 K^- \pi^+ \pi^-$	4580 ± 215
$D_s^+ \to K_S^0 K^- \pi^+ \pi^+$	9156 ± 182	$D_s^- \to K_S^0 K^+ \pi^- \pi^-$	8904 ± 181
$D_s^+ \to \pi^+ \pi^+ \pi^-$	20655 ± 444	$D_s^- \to \pi^+ \pi^- \pi^-$	20875 ± 446
$D_s^+ \to \pi^+ \eta_{\gamma\gamma}$	10755 ± 225	$D_s^- \to \pi^- \eta_{\gamma\gamma}$	11131 ± 226
$D_s^+ \to \pi^+ \pi^0 \eta_{\gamma\gamma}$	24551 ± 649	$D_s^- \to \pi^- \pi^0 \eta_{\gamma\gamma}$	24050 ± 648
$D_s^+ \to \pi^+ \pi^+ \pi^- \eta_{\gamma\gamma}$	6140 ± 319	$D_s^- \to \pi^+ \pi^- \pi^- \eta_{\gamma\gamma}$	6215 ± 320
$D_s^+ \to \pi^+ \eta_{\pi^+\pi^-\pi^0}$	2898 ± 88	$D_s^- \to \pi^- \eta_{\pi^+\pi^-\pi^0}$	2914 ± 87
$D_s^+ \to \pi^+ \eta'_{\pi^+\pi^-\eta_{\gamma\gamma}}$	5287 ± 99	$D_s^- \to \pi^- \eta'_{\pi^+\pi^-\eta_{\gamma\gamma}}$	5239 ± 99
$D_s^+ \to \pi^+ \pi^0 \eta'_{\pi^+\pi^-\eta_{\gamma\gamma}}$	2326 ± 136	$D_s^- \to \pi^- \pi^0 \eta'_{\pi^+\pi^-\eta_{\gamma\gamma}}$	2197 ± 139
$D_s^+ \to \pi^+ \eta'_{\pi^+\pi^-\eta_{\pi^+\pi^-\pi^0}}$	624 ± 33	$D_s^- \to \pi^- \eta'_{\pi^+\pi^-\eta_{\pi^+\pi^-\pi^0}}$	609 ± 33
$D_s^+ \to \pi^+ \eta'_{\rho\gamma}$	13192 ± 359	$D_s^- \to \pi^- \eta'_{\rho\gamma}$	14042 ± 362
$D_s^+ \to \pi^+ \pi^0 \eta'_{\rho\gamma}$	5156 ± 468	$D_s^- \to \pi^- \pi^0 \eta'_{\rho\gamma}$	5859 ± 471
$D_s^+ \to K_S^0 \pi^+ \pi^0$	1910 ± 172	$D_s^- \to K_S^0 \pi^- \pi^0$	1703 ± 171
$D_s^+ \to K^+ \pi^+ \pi^-$	10589 ± 394	$D_s^- \to K^- \pi^+ \pi^-$	9991 ± 390

Table 2. ST yields in data with statistical uncertainties at $\sqrt{s} = 4.178\,\mathrm{GeV}$.

numbers of events for nineteen final states of seven data samples in the signal region and the sideband regions are 42965 and 14728, respectively.

The DT backgrounds have two main components: a uniform background and the crossfeed background. Based on the fact that the inclusive MC samples adequately describe the data sample, we estimate the uniform background by using inclusive MC samples to derive a scale factor f for the uniform background as:

$$N_{\mathrm{bkg}} = f \times N_{\mathrm{sideband}}, \tag{5.1}$$

where N_{bkg} is the number of the uniform background events in the signal region and N_{sideband} is the number of the uniform background events in the sideband regions. To describe the crossfeed background, we use a method analogous to the one used for the ST crossfeed to create an efficiency-correction matrix, $\mathbf{C}^{\mathrm{DT}}$, and include this matrix in the BF fit.

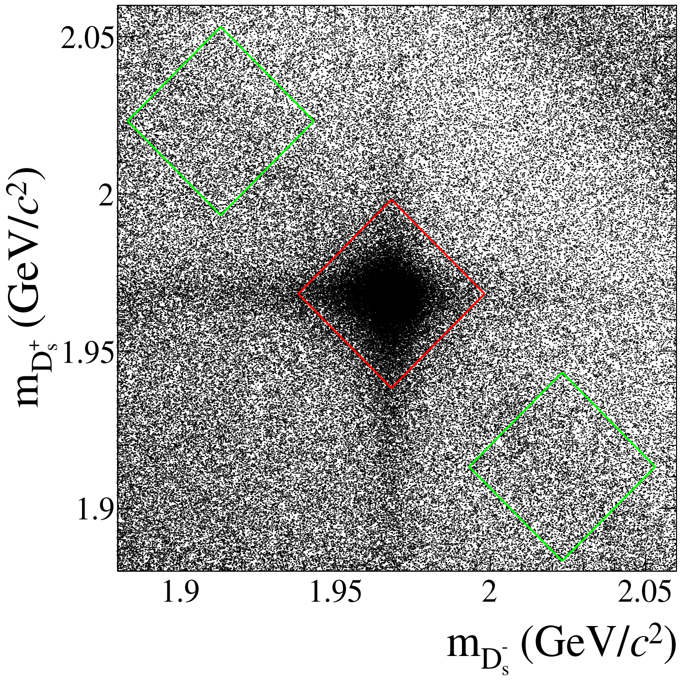

Figure 3. Invariant mass of the D_s^+ candidate versus invariant mass of the D_s^- candidate for all 361 DT final states and seven data samples. The squares show the signal region (red) and two sideband regions (green). There are 42965 events in the signal region and 14728 in the combined sideband regions.

6 Systematic uncertainties

The systematic uncertainties in the BF measurements mainly come from tracking and PID efficiencies, γ, K_S^0, π^0, and η reconstruction, intermediate decays, amplitude model, MC statistics, background shape, crossfeed probabilities and the scale factor from the uniform background distribution of DT yields. The efficiency systematics accounts for the momentum distributions of the relevant particles. We discuss each of them in detail below.

- $\pi^\pm$, $K^\pm$ tracking efficiency. The decays $e^+e^- \to K^+K^-K^+K^-$, $K^+K^-\pi^+\pi^-$ (π^0), and $\pi^+\pi^-\pi^+\pi^-$ (π^0) are used to study the K^+ and $\pi^\pm$ tracking efficiencies. The π^+ (π^-) and K^+ (K^-) data-MC tracking efficiency ratios, including the $\pi^\pm$ from $\eta_{\pi^+\pi^-\pi^0}$, $\eta'_{\pi^+\pi^-\pi^0}$ and $\rho(770)^0$, are given in table 3.

- $\pi^\pm$, $K^\pm$ PID efficiency. The $\pi^\pm/K^\pm$ PID efficiency is studied with the same control samples as the tracking efficiency. The π^+ (π^-) and K^+ (K^-) data-MC PID efficiency ratios, including the $\pi^\pm$ from $\eta_{\pi^+\pi^-\pi^0}$, $\eta'_{\pi^+\pi^-\pi^0}$ and $\rho(770)^0$, are given in table 3.

- K_S^0 reconstruction. The uncertainty for the K_S^0 reconstruction efficiency is studied using the control samples of $J/\psi \to K_S^0 K^+\pi^-$ and $\phi K_S^0 K^+\pi^-$ decays [41]. The data-MC K_S^0 reconstruction efficiency ratios are given in table 3.

- π^0 and $\eta_{\gamma\gamma}$ reconstruction. The systematic uncertainty associated with the π^0 reconstruction efficiency is investigated by using a control sample of the process $e^+e^- \to$

Final state	Tracking	PID	K_S^0	$\pi^0 \to \gamma\gamma$ ($\eta \to \gamma\gamma$)
$K_S^0 K^+$	1.001 ± 0.002	1.000 ± 0.002	1.020 ± 0.005	—
$K^+ K^- \pi^+$	1.007 ± 0.010	0.983 ± 0.006	—	—
$K_S^0 K^+ \pi^0$	1.002 ± 0.002	0.996 ± 0.002	1.028 ± 0.006	1.014 ± 0.010
$K_S^0 K_S^0 \pi^+$	0.995 ± 0.004	0.995 ± 0.002	1.056 ± 0.013	—
$K^+ K^- \pi^+ \pi^0$	1.010 ± 0.015	0.976 ± 0.006	—	1.017 ± 0.010
$K_S^0 K^+ \pi^+ \pi^-$	1.003 ± 0.011	0.986 ± 0.006	1.035 ± 0.008	—
$K_S^0 K^- \pi^+ \pi^+$	1.003 ± 0.011	0.987 ± 0.006	1.034 ± 0.008	—
$\pi^+ \pi^+ \pi^-$	1.005 ± 0.006	0.991 ± 0.006	—	—
$\pi^+ \eta$	1.002 ± 0.002	0.994 ± 0.002	—	0.987 ± 0.016
$\pi^+ \pi^0 \eta$	0.999 ± 0.002	0.996 ± 0.002	—	0.996 ± 0.020
$\pi^+ \pi^+ \pi^- \eta$	0.996 ± 0.007	0.992 ± 0.006	—	1.001 ± 0.010
$\pi^+ \eta_{3\pi}$	0.997 ± 0.007	0.989 ± 0.006	—	1.020 ± 0.010
$\pi^+ \eta'$	0.989 ± 0.011	0.984 ± 0.006	—	0.999 ± 0.010
$\pi^+ \pi^0 \eta'$	0.980 ± 0.013	0.981 ± 0.006	—	1.025 ± 0.020
$\pi^+ \eta'_{\pi^+\pi^-\eta_{3\pi}}$	0.973 ± 0.021	0.971 ± 0.010	—	1.033 ± 0.018
$\pi^+ \eta'_{\rho\gamma}$	1.002 ± 0.006	0.992 ± 0.006	—	—
$\pi^+ \pi^0 \eta'_{\rho\gamma}$	1.001 ± 0.006	0.994 ± 0.006	—	1.009 ± 0.010
$K_S^0 \pi^+ \pi^0$	0.999 ± 0.002	0.997 ± 0.002	1.026 ± 0.006	1.005 ± 0.010
$K^+ \pi^+ \pi^-$	1.005 ± 0.007	0.990 ± 0.006	—	—

Table 3. The data-MC efficiency ratios. The MC efficiencies have been corrected to data by these ratios and the uncertainties of the ratios are assigned as the systematic uncertainties. A "—" indicates that the ratio is not applicable.

$K^+K^-\pi^+\pi^-\pi^0$. The systematic uncertainty for $\eta_{\gamma\gamma}$ reconstruction is assigned to be the same vs. momentum as that of π^0 reconstruction. The average ratio between data and MC efficiencies of π^0 and $\eta_{\gamma\gamma}$ reconstruction, weighted by the corresponding momentum spectra are given in table 3.

- γ reconstruction. The systematic uncertainty of γ detection efficiency is 1% per photon, obtained by studying the control sample of $J/\psi \to \rho(770)^0\pi^0$ [42].

- Intermediate resonance decays. The uncertainties in the BFs of intermediate resonance decays are considered, as listed in the PDG [23]:

  - $\mathcal{B}$ $(K_S^0 \to \pi^+\pi^-) = (69.20 \pm 0.05)\%$,
  - $\mathcal{B}$ $(\pi^0 \to \gamma\gamma) = (98.823 \pm 0.034)\%$,

Final state	γ reconstruction	Intermediate resonance decay	Amplitude model
$K_S^0K^+$	—	0.07	—
$K^+K^-\pi^+$	—	—	0.50
$K_S^0K^+\pi^0$	—	0.08	0.80
$K_S^0K_S^0\pi^+$	—	0.14	0.50
$K^+K^-\pi^+\pi^0$	—	0.03	0.40
$K_S^0K^+\pi^+\pi^-$	—	0.07	0.40
$K_S^0K^-\pi^+\pi^+$	—	0.07	0.60
$\pi^+\pi^+\pi^-$	—	—	0.50
$\pi^+\eta_{\gamma\gamma}$	—	0.51	—
$\pi^+\pi^0\eta_{\gamma\gamma}$	—	0.51	0.60
$\pi^+\pi^+\pi^-\eta_{\gamma\gamma}$	—	0.51	0.40
$\pi^+\eta_{\pi^+\pi^-\pi^0}$	—	1.01	—
$\pi^+\eta'_{\pi^+\pi^-\eta_{\gamma\gamma}}$	—	1.28	—
$\pi^+\pi^0\eta'_{\pi^+\pi^-\eta_{\gamma\gamma}}$	—	1.28	0.40
$\pi^+\eta'_{\pi^+\pi^-\eta_{\pi^+\pi^-\pi^0}}$	—	1.18	—
$\pi^+\eta'_{\rho\gamma}$	1.00	1.36	—
$\pi^+\pi^0\eta'_{\rho\gamma}$	1.00	1.36	0.50
$K_S^0\pi^+\pi^0$	—	0.08	0.80
$K^+\pi^+\pi^-$	—	—	0.50

Table 4. Systematic uncertainties from γ reconstruction, intermediate resonance decays and amplitude model for the BF measurement (%). The "—" indicates that the uncertainty is not applicable.

- $\mathcal{B}(\eta \to \gamma\gamma) = (39.41 \pm 0.20)\%$,
- $\mathcal{B}(\eta \to \pi^+\pi^-\pi^0) = (22.68 \pm 0.23)\%$,
- $\mathcal{B}(\eta' \to \pi^+\pi^-\eta) = (42.5 \pm 0.5)\%$,
- $\mathcal{B}(\eta' \to \rho(770)^0\gamma) = (29.5 \pm 0.4)\%$.

- Amplitude model. The uncertainties from the amplitude models are estimated by varying the amplitude model parameters based on their error matrix. Here we assign the uncertainty according to the amplitude [26–36] as listed in table 4.

- MC statistics. The systematic uncertainties due to MC statistics arise from the statistical uncertainties of 266 ST and 2527 DT efficiencies. The total uncertainty from MC statistics for each mode is given in table 5.

JHEP05(2024)335

Final state	MC statistics	Background shape	Crossfeed probabilities	DT background factor
$K_S^0K^+$	0.10	0.01	0.01	0.01
$K^+K^-\pi^+$	0.05	0.01	0.00	0.01
$K_S^0K^+\pi^0$	0.15	0.07	0.01	0.07
$K_S^0K_S^0\pi^+$	0.26	0.07	0.01	0.07
$K^+K^-\pi^+\pi^0$	0.08	0.04	0.00	0.04
$K_S^0K^+\pi^+\pi^-$	0.18	0.12	0.01	0.12
$K_S^0K^-\pi^+\pi^+$	0.14	0.05	0.00	0.05
$\pi^+\pi^+\pi^-$	0.09	0.06	0.01	0.06
$\pi^+\eta$	0.13	0.03	0.00	0.03
$\pi^+\pi^0\eta$	0.08	0.04	0.00	0.04
$\pi^+\pi^+\pi^-\eta$	0.16	0.13	0.01	0.13
$\pi^+\eta_{3\pi}$	0.25	0.05	0.01	0.05
$\pi^+\eta'$	0.18	0.02	0.00	0.02
$\pi^+\pi^0\eta'$	0.27	0.10	0.00	0.10
$\pi^+\eta'_{\pi^+\pi^-\eta_{3\pi}}$	0.50	0.05	0.00	0.05
$\pi^+\eta'_{\rho\gamma}$	0.12	0.05	0.00	0.05
$\pi^+\pi^0\eta'_{\rho\gamma}$	0.21	0.19	0.01	0.19
$K_S^0\pi^+\pi^0$	0.35	0.20	0.01	0.20
$K^+\pi^+\pi^-$	0.12	0.07	0.00	0.07

Table 5. Total systematic uncertainties from each of these sources: MC statistics, background shape, crossfeed probabilities and the scale factor from uniform background of DT yields for the BF measurement (%).

- Background shape. To estimate the uncertainty due to the background shape of the signal D_s^+ invariant mass distribution, the MC background shape is used to replace the second-order polynomial. The total uncertainty of the background shape for each mode is given in table 5.
- Crossfeed probabilities. The systematic uncertainty due to crossfeed probabilities is obtained by propagating the statistical uncertainties of the $\mathbf{C}^{\mathrm{ST}}$ and $\mathbf{C}^{\mathrm{DT}}$ matrices. The total uncertainty from crossfeed probabilities for each mode is given in table 5.
- The scale factor from uniform background of DT yields. The systematic uncertainty due to the scale factor from uniform background of DT yields is taken as the statistical uncertainty of f from the inclusive MC sample. The total uncertainty of the scale factor from uniform background of DT yields for each mode is given in table 5.

JHEP05(2024)335

For the data-MC efficiency ratios in table 3, the MC efficiencies have been corrected by these ratios and the uncertainties of the ratios are assigned to be the systematic uncertainties.

7 Branching fraction measurement

We use a maximum-likelihood fit to obtain the BFs and the number of $D_s^+D_s^-$ pairs by the observed ST and DT yields.

For the data sample k, we denote the number of $D_s^+D_s^-$ pairs as $N_k^{D_s^+D_s^-}$, the observed ST yield matrix as $\mathbf{N}_k^{\mathrm{ST}}$ (1×38 matrix) and the expected yield matrix $\mathbf{Y}_k^{\mathrm{ST}}$ (38×1 matrix):

$$\mathbf{Y}_k^{\mathrm{ST}} = N_k^{D_s^+D_s^-}\mathcal{B}^{\mathrm{ST}}\mathbf{C}_k^{\mathrm{ST}}, \tag{7.1}$$

where $\mathcal{B}^{\mathrm{ST}}$ (1×38 matrix) is the BF matrix and $\mathbf{C}_k^{\mathrm{ST}}$ (38×38 matrix) is the ST efficiency-correction matrix. The likelihood function of ST yields for data sample k ($\mathcal{L}_k^{\mathrm{ST}}$) can be expressed as:

$$\mathcal{L}_k^{\mathrm{ST}} = \frac{1}{\sqrt{2\pi\left|\det\mathbf{V}_k^{\mathrm{ST}}\right|}}\exp\left[(\mathbf{Y}_k^{\mathrm{ST}}-\mathbf{N}_k^{\mathrm{ST}})(\mathbf{V}_k^{\mathrm{ST}})^{-1}(\mathbf{Y}_k^{\mathrm{ST}}-\mathbf{N}_k^{\mathrm{ST}})^T/2\right], \tag{7.2}$$

where T is the transpose operation of a matrix, det is the determinant operation for a matrix, and $\mathbf{V}_k^{\mathrm{ST}}$ (38×38 matrix) is the ST statistical uncertainty matrix [40]:

$$V_{k,ij}^{\mathrm{ST}} = \begin{cases}\sigma_{\mathrm{ST},i}\sigma_{\mathrm{ST},j}, & i=j\\ \sigma^2_{\mathrm{DT},ij}, & i\neq j.\end{cases} \tag{7.3}$$

The diagonal elements are the statistical uncertainty of ST yields ($\sigma_{\mathrm{ST},i}$) and the off-diagonal elements are evaluated as the observed DT yield ($\sigma_{\mathrm{DT},ij}$). Since any event can contain both ST and DT candidates, the ST yields are correlated among themselves as well as with DT yields.

For a DT final state, $D_s^+\to i$ and $D_s^-\to\bar{j}$, in data sample k, we denote the observed DT yield in sideband regions as $S_{i,\bar{j},k}^{\mathrm{DT}}$ and the observed DT yield in the signal region as $N_{i,\bar{j},k}^{\mathrm{DT}}$. The expected yield at generator level is $\tilde{E}_{i,\bar{j},k}^{\mathrm{DT}}$:

$$\tilde{E}_{i,\bar{j},k}^{\mathrm{DT}} = N_k^{D_s^+D_s^-}\mathcal{B}_i\mathcal{B}_{\bar{j}}. \tag{7.4}$$

Based on eq. (7.4), we denote an expected yield matrix $\tilde{\mathbf{E}}_k^{\mathrm{DT}}$ (1×361 matrix) and an efficiency-corrected expected yield matrix $\mathbf{Y}_k^{\mathrm{DT}}$ (1×361 matrix) as:

$$\mathbf{Y}_k^{\mathrm{DT}} = \tilde{\mathbf{E}}_k^{\mathrm{DT}}\mathbf{C}_k^{\mathrm{DT}}, \tag{7.5}$$

where $\mathbf{C}_k^{\mathrm{DT}}$ (361×361 matrix) is the DT efficiency-correction matrix constructed in section 5.

The DT likelihood function $\mathcal{L}_{i,\bar{j},k}^{\mathrm{DT}}$ is given by the usual description of a Poisson signal in the presence of Poisson background [43]:

$$\begin{aligned}&\mathcal{L}_{i,\bar{j},k}^{\mathrm{DT}}(N_{i,\bar{j},k}^{\mathrm{DT}}, S_{i,\bar{j},k}^{\mathrm{DT}}; Y_{i,\bar{j},k}^{\mathrm{DT}}, \tilde{S}_{i,\bar{j},k}^{\mathrm{DT}}) =\\ &\quad\frac{1}{(N_{i,\bar{j},k}^{\mathrm{DT}})!}\frac{(Y_{i,\bar{j},k}^{\mathrm{DT}}+f_{i,\bar{j},k}\tilde{S}_{i,\bar{j},k}^{\mathrm{DT}})^{N_{i,\bar{j},k}^{\mathrm{DT}}}}{\exp(Y_{i,\bar{j},k}^{\mathrm{DT}}+f_{i,\bar{j},k}\tilde{S}_{i,\bar{j},k}^{\mathrm{DT}})}\frac{1}{(f_{i,\bar{j},k}S_{i,\bar{j},k}^{\mathrm{DT}})!}\frac{(f_{i,\bar{j},k}\tilde{S}_{i,\bar{j},k}^{\mathrm{DT}})^{(f_{i,\bar{j},k}S_{i,\bar{j},k}^{\mathrm{DT}})}}{\exp(f_{i,\bar{j},k}\tilde{S}_{i,\bar{j},k}^{\mathrm{DT}})},\end{aligned} \tag{7.6}$$

Mode	$\mathcal{B}$ (%)	PDG $\mathcal{B}$ (%)
$D_s^+ \to K_S^0 K^+$	$1.502 \pm 0.012 \pm 0.009$	1.453 ± 0.035
$D_s^+ \to K^+ K^- \pi^+$	$5.49 \pm 0.04 \pm 0.07$	5.37 ± 0.10
$D_s^+ \to K_S^0 K^+ \pi^0$	$1.47 \pm 0.02 \pm 0.02$	1.47 ± 0.07
$D_s^+ \to K_S^0 K_S^0 \pi^+$	$0.73 \pm 0.01 \pm 0.01$	0.71 ± 0.04
$D_s^+ \to K^+ K^- \pi^+ \pi^0$	$5.50 \pm 0.05 \pm 0.11$	5.50 ± 0.24
$D_s^+ \to K_S^0 K^+ \pi^+ \pi^-$	$0.93 \pm 0.02 \pm 0.01$	0.95 ± 0.08
$D_s^+ \to K_S^0 K^- \pi^+ \pi^+$	$1.56 \pm 0.02 \pm 0.02$	1.53 ± 0.08
$D_s^+ \to \pi^+ \pi^+ \pi^-$	$1.09 \pm 0.01 \pm 0.01$	1.08 ± 0.04
$D_s^+ \to \pi^+ \eta$	$1.69 \pm 0.02 \pm 0.02$	1.67 ± 0.09
$D_s^+ \to \pi^+ \pi^0 \eta$	$9.10 \pm 0.09 \pm 0.15$	9.5 ± 0.5
$D_s^+ \to \pi^+ \pi^+ \pi^- \eta$	$3.08 \pm 0.06 \pm 0.05$	3.12 ± 0.16
$D_s^+ \to \pi^+ \eta'$	$3.95 \pm 0.04 \pm 0.07$	3.94 ± 0.25
$D_s^+ \to \pi^+ \pi^0 \eta'$	$6.17 \pm 0.12 \pm 0.14$	6.08 ± 0.29
$D_s^+ \to K_S^0 \pi^+ \pi^0$	$0.51 \pm 0.02 \pm 0.01$	0.54 ± 0.03
$D_s^+ \to K^+ \pi^+ \pi^-$	$0.620 \pm 0.009 \pm 0.006$	0.620 ± 0.019

Table 6. Results of the BF fit and comparison to the PDG values. For results in this paper, the first uncertainties are statistical and the second ones systematic. For the PDG total uncertainties are shown.

where $f_{i,\bar{j},k}$ is the scale factor from uniform background of DT yields in eq. (5.1) and $\tilde{S}^{\rm DT}_{i,\bar{j},k}$ is the expected yield in sideband regions and eliminated by solving $\partial(\mathcal{L}^{\rm DT}_{i,\bar{j},k})/\partial\tilde{S}^{\rm DT}_{i,\bar{j},k} = 0$ analytically.

Based on seven data samples and 19×19 DT final states, the final likelihood function ($\mathcal{L}$) can be expressed as:

$$\mathcal{L} = \prod_{k=1}^{7} \mathcal{L}_k^{\rm ST} \prod_{i=1}^{19} \prod_{\bar{j}=1}^{19} \mathcal{L}^{\rm DT}_{i,\bar{j},k}. \tag{7.7}$$

The results of the BF fit and comparisons to the PDG [23] are listed in table 6. The fitted numbers of produced $D_s^+ D_s^-$ pairs for seven data samples are list in table 7.

We check the internal consistency of the BF fitting procedure using the inclusive MC sample, which corresponds to an integrated luminosity of 40 times the recorded data set, and find that central values and pull distributions for the fitted parameters are reasonable.

Systematic uncertainties are propagated to the final results by adjusting fit inputs, including efficiencies, ST yields, DT yields in the signal region and the sideband regions and scale factors from uniform background of DT yields. The appropriate correlations are included using the detailed results of section 6. The uncertainties from tracking and PID efficiencies, intermediate decays, amplitude model and the K_S^0, π^0, η, and γ reconstruction

JHEP05(2024)335

$\sqrt{s}$ (GeV)	$N^{D_s^+ D_s^-}$ ($\times 10^5$)
4.128 and 4.157	$6.29 \pm 0.06 \pm 0.01$
4.178	$31.79 \pm 0.24 \pm 0.06$
4.189	$5.51 \pm 0.05 \pm 0.01$
4.199	$4.92 \pm 0.05 \pm 0.01$
4.209	$5.07 \pm 0.05 \pm 0.01$
4.219	$4.32 \pm 0.04 \pm 0.01$
4.226	$6.82 \pm 0.07 \pm 0.02$

Table 7. The numbers of produced $D_s^+ D_s^-$ pairs for the seven data samples. The first and second uncertainties are statistical and systematic uncertainties, respectively.

are correlated while the uncertainties from MC statistics, ST background shape, crossfeed probabilities and the background of DT yields are uncorrelated.

For each correlated systematic uncertainty, we change all corresponding input values of all ST final states and DT final states with the expected systematic in that mode and obtain the new fit values. For each uncorrelated systematic uncertainty from every final state, we only change the corresponding input value of that final state with the expected systematics. For each parameter, the changes in the fitted value are taken as the contribution to the systematic uncertainty, and the sum of all contributions in quadrature gives the total systematic uncertainty.

8 *CP* asymmetries measurement

We derive the CP asymmetry for each mode by:

$$\mathcal{A}_{CP,i} = \frac{\sum_{k=1}^{7}(N_{i,k}^{\rm ST}/\epsilon_{i,k}^{\rm ST} - N_{\bar{i},k}^{\rm ST}/\epsilon_{\bar{i},k}^{\rm ST})}{\sum_{k=1}^{7}(N_{i,k}^{\rm ST}/\epsilon_{i,k}^{\rm ST} + N_{\bar{i},k}^{\rm ST}/\epsilon_{\bar{i},k}^{\rm ST})}, \tag{8.1}$$

where $N_{i,k}^{\rm ST}$ and $\epsilon_{i,k}^{\rm ST}$ ($N_{\bar{i},k}^{\rm ST}$ and $\epsilon_{\bar{i},k}^{\rm ST}$) are the yields and efficiencies for the ST mode i ($\bar{i}$) from date sample k. Almost all systematic uncertainties cancel in $\mathcal{A}_{CP}$ calculations, except the ST efficiency statistical uncertainty, the ST yield fit uncertainties, and the uncertainties from tracking efficiencies. The results of the $\mathcal{A}_{CP}$ calculation and comparison to the PDG [23] are listed in table 8.

9 Summary

We have measured the absolute BFs for fifteen hadronic D_s^+ decays, reconstructed in nineteen final states, using a sample of e^+e^- collision data corresponding to an integrated luminosity of 7.33 fb^{-1} collected with the BESIII detector at center-of-mass energies between 4.128 and 4.226 GeV. The BFs obtained and shown in table 6 are in agreement with the world-average values [23], but typically with much improved precision. The BFs of selected important

JHEP05(2024)335

Mode	$\mathcal{A}_{CP}$ (%)	PDG $\mathcal{A}_{CP}$ (%)
$D_s^\pm \to K_S^0 K^\pm$	$0.29 \pm 0.50 \pm 0.21$	0.09 ± 0.26
$D_s^\pm \to K^+ K^- \pi^\pm$	$0.48 \pm 0.26 \pm 0.24$	-0.5 ± 0.9
$D_s^\pm \to K_S^0 K^\pm \pi^0$	$-0.85 \pm 1.97 \pm 0.46$	-2 ± 6
$D_s^\pm \to K_S^0 K_S^0 \pi^\pm$	$1.14 \pm 1.58 \pm 0.44$	3 ± 5
$D_s^\pm \to K^+ K^- \pi^\pm \pi^0$	$-0.66 \pm 0.91 \pm 0.33$	0.0 ± 3.0
$D_s^\pm \to K_S^0 K^\pm \pi^+ \pi^-$	$2.00 \pm 2.37 \pm 0.70$	-6 ± 5
$D_s^\pm \to K_S^0 K^\mp \pi^\pm \pi^\pm$	$-0.24 \pm 1.05 \pm 1.07$	4.1 ± 2.8
$D_s^\pm \to \pi^\pm \pi^+ \pi^-$	$-0.88 \pm 1.17 \pm 0.38$	-0.7 ± 3.1
$D_s^\pm \to \pi^\pm \eta$	$-0.44 \pm 0.89 \pm 0.19$	0.3 ± 0.4
$D_s^\pm \to \pi^\pm \pi^0 \eta$	$1.05 \pm 1.45 \pm 0.62$	-1 ± 4
$D_s^\pm \to \pi^\pm \pi^+ \pi^- \eta$	$2.42 \pm 2.85 \pm 0.78$	-
$D_s^\pm \to \pi^\pm \eta'$	$-0.59 \pm 0.76 \pm 0.20$	-0.9 ± 0.5
$D_s^\pm \to \pi^\pm \pi^0 \eta'$	$-1.60 \pm 2.57 \pm 0.64$	0 ± 8
$D_s^\pm \to K_S^0 \pi^\pm \pi^0$	$-2.17 \pm 4.65 \pm 1.10$	3 ± 6
$D_s^\pm \to K^\pm \pi^+ \pi^-$	$1.81 \pm 2.01 \pm 0.45$	4 ± 5

Table 8. Results of the $\mathcal{A}_{CP}$ calculation for this paper and comparison to the PDG. For results in this paper, the first uncertainties are statistical and the second ones systematic. For the PDG total uncertainties are shown.

reference modes are:

$$
\begin{aligned}
\mathcal{B}(D_s^+ \to K^+ K^- \pi^+) &= (5.49 \pm 0.04 \pm 0.07)\%, \\
\mathcal{B}(D_s^+ \to K_S^0 K^+) &= (1.50 \pm 0.01 \pm 0.01)\%, \\
\mathcal{B}(D_s^+ \to K^+ K^- \pi^+ \pi^0) &= (5.50 \pm 0.05 \pm 0.11)\%,
\end{aligned}
$$

where the first uncertainties are statistical and the second are systematic. Additionally, the CP-violating asymmetries of the fifteen hadronic $D_s^\pm$ decays are measured. No significant asymmetries are observed.

Acknowledgments

The BESIII collaboration thanks the staff of BEPCII and the IHEP computing center for their strong support. This work is supported in part by National Key R&D Program of China under Contracts Nos. 2020YFA0406400, 2020YFA0406300; National Natural Science Foundation of China (NSFC) under Contracts Nos. 11635010, 11735014, 11835012, 11935015, 11935016, 11935018, 11961141012, 12025502, 12035009, 12035013, 12061131003, 12192260, 12192261, 12192262, 12192263, 12192264, 12192265, 12221005, 12225509, 12235017; the

Chinese Academy of Sciences (CAS) Large-Scale Scientific Facility Program; the CAS Center for Excellence in Particle Physics (CCEPP); Joint Large-Scale Scientific Facility Funds of the NSFC and CAS under Contract No. U1832207; CAS Key Research Program of Frontier Sciences under Contracts Nos. QYZDJ-SSW-SLH003, QYZDJ-SSW-SLH040; 100 Talents Program of CAS; The Institute of Nuclear and Particle Physics (INPAC) and Shanghai Key Laboratory for Particle Physics and Cosmology; European Union's Horizon 2020 research and innovation programme under Marie Sklodowska-Curie grant agreement under Contract No. 894790; German Research Foundation DFG under Contracts Nos. 455635585, Collaborative Research Center CRC 1044, FOR5327, GRK 2149; Istituto Nazionale di Fisica Nucleare, Italy; Ministry of Development of Turkey under Contract No. DPT2006K-120470; National Research Foundation of Korea under Contract No. NRF-2022R1A2C1092335; National Science and Technology fund of Mongolia; National Science Research and Innovation Fund (NSRF) via the Program Management Unit for Human Resources & Institutional Development, Research and Innovation of Thailand under Contract No. B16F640076; Polish National Science Centre under Contract No. 2019/35/O/ST2/02907; The Swedish Research Council; U.S. Department of Energy under Contract No. DE-FG02-05ER41374.

References

[1] H.-Y. Cheng, C.-W. Chiang and Z.-Q. Zhang, *Hadronic three-body D decays mediated by scalar resonances*, Phys. Rev. D **105** (2022) 033006 [arXiv:2201.00460] [INSPIRE].

[2] H.-Y. Cheng, C.-W. Chiang and Z.-Q. Zhang, *Two- and three-body hadronic decays of charmed mesons involving a tensor meson*, Phys. Rev. D **105** (2022) 093006 [arXiv:2203.04561] [INSPIRE].

[3] H.-Y. Cheng and C.-W. Chiang, *Revisiting CP violation in $D \to PP$ and VP decays*, Phys. Rev. D **100** (2019) 093002 [arXiv:1909.03063] [INSPIRE].

[4] Q. Qin, H.-N. Li, C.-D. Lü and F.-S. Yu, *Branching ratios and direct CP asymmetries in $D \to PV$ decays*, Phys. Rev. D **89** (2014) 054006 [arXiv:1305.7021] [INSPIRE].

[5] H.-N. Li, C.-D. Lü and F.-S. Yu, *Branching ratios and direct CP asymmetries in $D \to PP$ decays*, Phys. Rev. D **86** (2012) 036012 [arXiv:1203.3120] [INSPIRE].

[6] Y. Fu-Sheng, X.-X. Wang and C.-D. Lü, *Nonleptonic Two Body Decays of Charmed Mesons*, Phys. Rev. D **84** (2011) 074019 [arXiv:1101.4714] [INSPIRE].

[7] B. Bhattacharya and J.L. Rosner, *Charmed meson decays to two pseudoscalars*, Phys. Rev. D **81** (2010) 014026 [arXiv:0911.2812] [INSPIRE].

[8] B. Bhattacharya and J.L. Rosner, *Decays of Charmed Mesons to PV Final States*, Phys. Rev. D **79** (2009) 034016 [*Erratum ibid.* **81** (2010) 099903] [arXiv:0812.3167] [INSPIRE].

[9] LHCb collaboration, *Measurement of $|V_{cb}|$ with $B_s^0 \to D_s^{(*)-}\mu^+\nu_\mu$ decays*, Phys. Rev. D **101** (2020) 072004 [arXiv:2001.03225] [INSPIRE].

[10] BESIII collaboration, *Design and Construction of the BESIII Detector*, Nucl. Instrum. Meth. A **614** (2010) 345 [arXiv:0911.4960] [INSPIRE].

JHEP05(2024)335

[11] CLEO collaboration, *Improved Measurement of Absolute Hadronic Branching Fractions of the D_s^+ Meson*, Phys. Rev. D **88** (2013) 032009 [arXiv:1306.5363] [INSPIRE].

[12] MARK-III collaboration, *Direct Measurements of Charmed d Meson Hadronic Branching Fractions*, Phys. Rev. Lett. **56** (1986) 2140 [INSPIRE].

[13] C. Yu et al., *BEPCII Performance and Beam Dynamics Studies on Luminosity*, in the proceedings of the *7th International Particle Accelerator Conference*, Busan, South Korea, 8–13 May 2016, JACoW Publishing, Geneva, Switzerland (2016), pp. 1014–1018 [DOI:10.18429/JACoW-IPAC2016-TUYA01] [INSPIRE].

[14] K.-X. Huang et al., *Method for detector description transformation to Unity and application in BESIII*, Nucl. Sci. Tech. **33** (2022) 142 [arXiv:2206.10117] [INSPIRE].

[15] X. Li, Y. Sun, C. Li et al., *Study of MRPC technology for BESIII endcap-TOF upgrade*, Radiat. Detect. Technol. Meth. **1** (2017) 13 [INSPIRE].

[16] Y.X. Guo, S.S. Sun, F.F. An et al., *The study of time calibration for upgraded end cap TOF of BESIII*, Radiat. Detect. Technol. Meth. **1** (2017) 15 [INSPIRE].

[17] P. Cao et al., *Design and construction of the new BESIII endcap Time-of-Flight system with MRPC Technology*, Nucl. Instrum. Meth. A **953** (2020) 163053 [INSPIRE].

[18] H.-B. Li and X.-R. Lyu, *Study of the standard model with weak decays of charmed hadrons at BESIII*, Natl. Sci. Rev. **8** (2021) nwab181 [arXiv:2103.00908] [INSPIRE].

[19] BESIII collaboration, *Precise measurement of the* $e^+e^- \to D_s^+ D_s^-$ *cross sections at center-of-mass energies from threshold to* 4.95 *GeV*, arXiv:2403.14998 [INSPIRE].

[20] BESIII collaboration, *Measurements of the center-of-mass energies of collisions at BESIII*, Chin. Phys. C **45** (2021) 103001 [arXiv:2012.14750] [INSPIRE].

[21] BESIII collaboration, *Measurement of integrated luminosities at BESIII for data samples at center-of-mass energies between* 4.0 *and* 4.6 *GeV*, Chin. Phys. C **46** (2022) 113002 [arXiv:2203.03133] [INSPIRE].

[22] GEANT4 collaboration, *GEANT4 — a simulation toolkit*, Nucl. Instrum. Meth. A **506** (2003) 250 [INSPIRE].

[23] Particle Data collaboration, *Review of Particle Physics*, Prog. Theor. Exp. Phys. **2022** (2022) 083C01 [INSPIRE].

[24] R.-G. Ping, *Event generators at BESIII*, Chin. Phys. C **32** (2008) 599 [INSPIRE].

[25] S. Jadach, B.F.L. Ward and Z. Waş, *Coherent exclusive exponentiation for precision Monte Carlo calculations*, Phys. Rev. D **63** (2001) 113009 [hep-ph/0006359] [INSPIRE].

[26] BESIII collaboration, *Amplitude analysis and branching fraction measurement of* $D_s^+ \to K^+K^-\pi^+$, Phys. Rev. D **104** (2021) 012016 [arXiv:2011.08041] [INSPIRE].

[27] BESIII collaboration, *Observation of an* a_0*-like State with Mass of* 1.817 *GeV in the Study of* $D_s^+ \to K_S^0 K^+ \pi^0$ *Decays*, Phys. Rev. Lett. **129** (2022) 182001 [arXiv:2204.09614] [INSPIRE].

[28] BESIII collaboration, *Study of the decay* $D_s^+ \to K_S^0 K_S^0 \pi^+$ *and observation an isovector partner to* $f_0(1710)$, Phys. Rev. D **105** (2022) L051103 [arXiv:2110.07650] [INSPIRE].

[29] BESIII collaboration, *Amplitude analysis and branching fraction measurement of* $D_s^+ \to K^-K^+\pi^+\pi^0$, Phys. Rev. D **104** (2021) 032011 [arXiv:2103.02482] [INSPIRE].

[30] BESIII collaboration, *Amplitude analysis and branching-fraction measurement of* $D_s^+ \to K_S^0 K^- \pi^+\pi^+$, Phys. Rev. D **103** (2021) 092006 [arXiv:2102.03808] [INSPIRE].

JHEP05(2024)335

[31] BESIII collaboration, *Amplitude analysis of $D_s^+ \to \pi^+\pi^-\pi^+$*, Phys. Rev. D **106** (2022) 112006 [arXiv:2108.10050] [INSPIRE].

[32] BESIII collaboration, *Amplitude analysis of $D_s^+ \to \pi^+\pi^0\eta$ and first observation of the pure W-annihilation decays $D_s^+ \to a_0(980)^+\pi^0$ and $D_s^+ \to a_0(980)^0\pi^+$*, Phys. Rev. Lett. **123** (2019) 112001 [arXiv:1903.04118] [INSPIRE].

[33] BESIII collaboration, *Study of the Decay $D_s^+ \to \pi^+\pi^+\pi^-\eta$ and Observation of the W-annihilation Decay $D_s^+ \to a_0(980)^+\rho^0$*, Phys. Rev. D **104** (2021) L071101 [arXiv:2106.13536] [INSPIRE].

[34] BESIII collaboration, *Amplitude analysis and branching-fraction measurement of $D_s^+ \to \pi^+\pi^0\eta'$*, JHEP **04** (2022) 058 [arXiv:2202.04232] [INSPIRE].

[35] BESIII collaboration, *Amplitude analysis and branching-fraction measurement of $D_s^+ \to K_S^0\pi^+\pi^0$*, JHEP **06** (2021) 181 [arXiv:2103.15098] [INSPIRE].

[36] BESIII collaboration, *Amplitude analysis and branching fraction measurement of the decay $D_s^+ \to K^+\pi^+\pi^-$*, JHEP **08** (2022) 196 [arXiv:2205.08844] [INSPIRE].

[37] R.-L. Yang, R.-G. Ping and H. Chen, *Tuning and Validation of the Lundcharm Model with J/ψ Decays*, Chin. Phys. Lett. **31** (2014) 061301 [INSPIRE].

[38] R.-G. Ping, *An exclusive event generator for e^+e^- scan experiments*, Chin. Phys. C **38** (2014) 083001 [arXiv:1309.3932] [INSPIRE].

[39] E. Richter-Was, *QED bremsstrahlung in semileptonic B and leptonic tau decays*, Phys. Lett. B **303** (1993) 163 [INSPIRE].

[40] W.M. Sun, *Simultaneous least squares treatment of statistical and systematic uncertainties*, Nucl. Instrum. Meth. A **556** (2006) 325 [physics/0503050] [INSPIRE].

[41] BESIII collaboration, *Study of decay dynamics and CP asymmetry in $D^+ \to K_L^0 e^+\nu_e$ decay*, Phys. Rev. D **92** (2015) 112008 [arXiv:1510.00308] [INSPIRE].

[42] BESIII collaboration, *Branching fraction measurements of χ_{c0} and χ_{c2} to $\pi^0\pi^0$ and $\eta\eta$*, Phys. Rev. D **81** (2010) 052005 [arXiv:1001.5360] [INSPIRE].

[43] J. Conrad, O. Botner, A. Hallgren and C. Perez de los Heros, *Including systematic uncertainties in confidence interval construction for Poisson statistics*, Phys. Rev. D **67** (2003) 012002 [hep-ex/0202013] [INSPIRE].

JHEP05(2024)335

The BESIII collaboration

M. Ablikim[1], M.N. Achasov[4,c], P. Adlarson[75], O. Afedulidis[3], X.C. Ai[80], R. Aliberti[35], A. Amoroso[74A,74C], Q. An[71,58,a], Y. Bai[57], O. Bakina[36], I. Balossino[29A], Y. Ban[46,h], H.-R. Bao[63], V. Batozskaya[1,44], K. Begzsuren[32], N. Berger[35], M. Berlowski[44], M. Bertani[28A], D. Bettoni[29A], F. Bianchi[74A,74C], E. Bianco[74A,74C], A. Bortone[74A,74C], I. Boyko[36], R.A. Briere[5], A. Brueggemann[68], H. Cai[76], X. Cai[1,58], A. Calcaterra[28A], G.F. Cao[1,63], N. Cao[1,63], S.A. Cetin[62A], J.F. Chang[1,58], G.R. Che[43], G. Chelkov[36,b], C. Chen[43], C.H. Chen[9], Chao Chen[55], G. Chen[1], H.S. Chen[1,63], H.Y. Chen[20], M.L. Chen[1,58,63], S.J. Chen[42], S.L. Chen[45], S.M. Chen[61], T. Chen[1,63], X.R. Chen[31,63], X.T. Chen[1,63], Y.B. Chen[1,58], Y.Q. Chen[34], Z.J. Chen[25,i], Z.Y. Chen[1,63], S.K. Choi[10], G. Cibinetto[29A], F. Cossio[74C], J.J. Cui[50], H.L. Dai[1,58], J.P. Dai[78], A. Dbeyssi[18], R.E. de Boer[3], D. Dedovich[36], C.Q. Deng[72], Z.Y. Deng[1], A. Denig[35], I. Denysenko[36], M. Destefanis[74A,74C], F. De Mori[74A,74C], B. Ding[66,1], X.X. Ding[46,h], Y. Ding[34], Y. Ding[40], J. Dong[1,58], L.Y. Dong[1,63], M.Y. Dong[1,58,63], X. Dong[76], M.C. Du[1], S.X. Du[80], Z.H. Duan[42], P. Egorov[36,b], Y.H. Fan[45], J. Fang[59], J. Fang[1,58], S.S. Fang[1,63], W.X. Fang[1], Y. Fang[1], Y.Q. Fang[1,58], R. Farinelli[29A], L. Fava[74B,74C], F. Feldbauer[3], G. Felici[28A], C.Q. Feng[71,58], J.H. Feng[59], Y.T. Feng[71,58], M. Fritsch[3], C.D. Fu[1], J.L. Fu[63], Y.W. Fu[1,63], H. Gao[63], X.B. Gao[41], Y.N. Gao[46,h], Yang Gao[71,58], S. Garbolino[74C], I. Garzia[29A,29B], L. Ge[80], P.T. Ge[76], Z.W. Ge[42], C. Geng[59], E.M. Gersabeck[67], A. Gilman[69], K. Goetzen[13], L. Gong[40], W.X. Gong[1,58], W. Gradl[35], S. Gramigna[29A,29B], M. Greco[74A,74C], M.H. Gu[1,58], Y.T. Gu[15], C.Y. Guan[1,63], Z.L. Guan[22], A.Q. Guo[31,63], L.B. Guo[41], M.J. Guo[50], R.P. Guo[49], Y.P. Guo[12,g], A. Guskov[36,b], J. Gutierrez[27], K.L. Han[63], T.T. Han[1], X.Q. Hao[19], F.A. Harris[65], K.K. He[55], K.L. He[1,63], F.H. Heinsius[3], C.H. Heinz[35], Y.K. Heng[1,58,63], C. Herold[60], T. Holtmann[3], P.C. Hong[34], G.Y. Hou[1,63], X.T. Hou[1,63], Y.R. Hou[63], Z.L. Hou[1], B.Y. Hu[59], H.M. Hu[1,63], J.F. Hu[56,j], S.L. Hu[12,g], T. Hu[1,58,63], Y. Hu[1], G.S. Huang[71,58], K.X. Huang[59], L.Q. Huang[31,63], X.T. Huang[50], Y.P. Huang[1], T. Hussain[73], F. Hölzken[3], N. Hüsken[27,35], N. in der Wiesche[68], J. Jackson[27], S. Janchiv[32], J.H. Jeong[10], Q. Ji[1], Q.P. Ji[19], W. Ji[1,63], X.B. Ji[1,63], X.L. Ji[1,58], Y.Y. Ji[50], X.Q. Jia[50], Z.K. Jia[71,58], D. Jiang[1,63], H.B. Jiang[76], P.C. Jiang[46,h], S.S. Jiang[39], T.J. Jiang[16], X.S. Jiang[1,58,63], Y. Jiang[63], J.B. Jiao[50], J.K. Jiao[34], Z. Jiao[23], S. Jin[42], Y. Jin[66], M.Q. Jing[1,63], X.M. Jing[63], T. Johansson[75], S. Kabana[33], N. Kalantar-Nayestanaki[64], X.L. Kang[9], X.S. Kang[40], M. Kavatsyuk[64], B.C. Ke[80], V. Khachatryan[27], A. Khoukaz[68], R. Kiuchi[1], O.B. Kolcu[62A], B. Kopf[3], M. Kuessner[3], X. Kui[1,63], N. Kumar[26], A. Kupsc[44,75], W. Kühn[37], J.J. Lane[67], P. Larin[18], L. Lavezzi[74A,74C], T.T. Lei[71,58], Z.H. Lei[71,58], M. Lellmann[35], T. Lenz[35], C. Li[43], C. Li[47], C.H. Li[39], Cheng Li[71,58], D.M. Li[80], F. Li[1,58], G. Li[1], H.B. Li[1,63], H.J. Li[19], H.N. Li[56,j], Hui Li[43], J.R. Li[61], J.S. Li[59], Ke Li[1], L.J. Li[1,63], L.K. Li[1], Lei Li[48], M.H. Li[43], P.R. Li[38,l], Q.M. Li[1,63], Q.X. Li[50], R. Li[17,31], S.X. Li[12], T. Li[50], W.D. Li[1,63], W.G. Li[1,a], X. Li[1,63], X.H. Li[71,58], X.L. Li[50], X.Z. Li[59], Xiaoyu Li[1,63], Y.G. Li[46,h], Z.J. Li[59], Z.X. Li[15], C. Liang[42], H. Liang[71,58], H. Liang[1,63], Y.F. Liang[54], Y.T. Liang[31,63], G.R. Liao[14], L.Z. Liao[50], J. Libby[26], A. Limphirat[60], C.C. Lin[55], D.X. Lin[31,63], T. Lin[1], B.J. Liu[1], B.X. Liu[76], C. Liu[34], C.X. Liu[1], F.H. Liu[53], Fang Liu[1], Feng Liu[6], G.M. Liu[56,j], H. Liu[38,k,l], H.B. Liu[15], H.M. Liu[1,63], Huanhuan Liu[1], Huihui Liu[21], J.B. Liu[71,58], J.Y. Liu[1,63], K. Liu[38,k,l], K.Y. Liu[40], Ke Liu[22], L. Liu[71,58], L.C. Liu[43], Lu Liu[43], M.H. Liu[12,g], P.L. Liu[1], Q. Liu[63], S.B. Liu[71,58], T. Liu[12,g], W.K. Liu[43], W.M. Liu[71,58], X. Liu[38,k,l], X. Liu[39], Y. Liu[80], Y. Liu[38,k,l], Y.B. Liu[43], Z.A. Liu[1,58,63], Z.D. Liu[9], Z.Q. Liu[50], X.C. Lou[1,58,63], F.X. Lu[59], H.J. Lu[23], J.G. Lu[1,58], X.L. Lu[1], Y. Lu[7], Y.P. Lu[1,58], Z.H. Lu[1,63], C.L. Luo[41], M.X. Luo[79], T. Luo[12,g], X.L. Luo[1,58], X.R. Lyu[63], Y.F. Lyu[43],

JHEP05(2024)335

F.C. Ma[40], H. Ma[78], H.L. Ma[1], J.L. Ma[1,63], L.L. Ma[50], M.M. Ma[1,63], Q.M. Ma[1], R.Q. Ma[1,63], X.T. Ma[1,63], X.Y. Ma[1,58], Y. Ma[46,h], Y.M. Ma[31], F.E. Maas[18], M. Maggiora[74A,74C], S. Malde[69], Y.J. Mao[46,h], Z.P. Mao[1], S. Marcello[74A,74C], Z.X. Meng[66], J.G. Messchendorp[13,64], G. Mezzadri[29A], H. Miao[1,63], T.J. Min[42], R.E. Mitchell[27], X.H. Mo[1,58,63], B. Moses[27], N.Yu. Muchnoi[4,c], J. Muskalla[35], Y. Nefedov[36], F. Nerling[18,e], L.S. Nie[20], I.B. Nikolaev[4,c], Z. Ning[1,58], S. Nisar[11,m], Q.L. Niu[38,k,l], W.D. Niu[55], Y. Niu[50], S.L. Olsen[63], Q. Ouyang[1,58,63], S. Pacetti[28B,28C], X. Pan[55], Y. Pan[57], A. Pathak[34], P. Patteri[28A], Y.P. Pei[71,58], M. Pelizaeus[3], H.P. Peng[71,58], Y.Y. Peng[38,k,l], K. Peters[13,e], J.L. Ping[41], R.G. Ping[1,63], S. Plura[35], V. Prasad[33], F.Z. Qi[1], H. Qi[71,58], H.R. Qi[61], M. Qi[42], T.Y. Qi[12,g], S. Qian[1,58], W.B. Qian[63], C.F. Qiao[63], X.K. Qiao[80], J.J. Qin[72], L.Q. Qin[14], L.Y. Qin[71,58], X.S. Qin[50], Z.H. Qin[1,58], J.F. Qiu[1], Z.H. Qu[72], C.F. Redmer[35], K.J. Ren[39], A. Rivetti[74C], M. Rolo[74C], G. Rong[1,63], Ch. Rosner[18], S.N. Ruan[43], N. Salone[44], A. Sarantsev[36,d], Y. Schelhaas[35], K. Schoenning[75], M. Scodeggio[29A], K.Y. Shan[12,g], W. Shan[24], X.Y. Shan[71,58], Z.J. Shang[38,k,l], J.F. Shangguan[55], L.G. Shao[1,63], M. Shao[71,58], C.P. Shen[12,g], H.F. Shen[1,8], W.H. Shen[63], X.Y. Shen[1,63], B.A. Shi[63], H. Shi[71,58], H.C. Shi[71,58], J.L. Shi[12,g], J.Y. Shi[1], Q.Q. Shi[55], S.Y. Shi[72], X. Shi[1,58], J.J. Song[19], T.Z. Song[59], W.M. Song[34,1], Y.J. Song[12,g], Y.X. Song[46,h,n], S. Sosio[74A,74C], S. Spataro[74A,74C], F. Stieler[35], Y.J. Su[63], G.B. Sun[76], G.X. Sun[1], H. Sun[63], H.K. Sun[1], J.F. Sun[19], K. Sun[61], L. Sun[76], S.S. Sun[1,63], T. Sun[51,f], W.Y. Sun[34], Y. Sun[9], Y.J. Sun[71,58], Y.Z. Sun[1], Z.Q. Sun[1,63], Z.T. Sun[50], C.J. Tang[54], G.Y. Tang[1], J. Tang[59], Y.A. Tang[76], L.Y. Tao[72], Q.T. Tao[25,i], M. Tat[69], J.X. Teng[71,58], V. Thoren[75], W.H. Tian[59], Y. Tian[31,63], Z.F. Tian[76], I. Uman[62B], Y. Wan[55], S.J. Wang[50], B. Wang[1], B.L. Wang[63], Bo Wang[71,58], D.Y. Wang[46,h], F. Wang[72], H.J. Wang[38,k,l], J.J. Wang[76], J.P. Wang[50], K. Wang[1,58], L.L. Wang[1], M. Wang[50], Meng Wang[1,63], N.Y. Wang[63], S. Wang[12,g], S. Wang[38,k,l], T. Wang[12,g], T.J. Wang[43], W. Wang[72], W. Wang[59], W.P. Wang[35,71,o], X. Wang[46,h], X.F. Wang[38,k,l], X.J. Wang[39], X.L. Wang[12,g], X.N. Wang[1], Y. Wang[61], Y.D. Wang[45], Y.F. Wang[1,58,63], Y.L. Wang[19], Y.N. Wang[45], Y.Q. Wang[1], Yaqian Wang[17], Yi Wang[61], Z. Wang[1,58], Z.L. Wang[72], Z.Y. Wang[1,63], Ziyi Wang[63], D.H. Wei[14], F. Weidner[68], S.P. Wen[1], Y.R. Wen[39], U. Wiedner[3], G. Wilkinson[69], M. Wolke[75], L. Wollenberg[3], C. Wu[39], J.F. Wu[1,8], L.H. Wu[1], L.J. Wu[1,63], X. Wu[12,g], X.H. Wu[34], Y. Wu[71,58], Y.H. Wu[55], Y.J. Wu[31], Z. Wu[1,58], L. Xia[71,58], X.M. Xian[39], B.H. Xiang[1,63], T. Xiang[46,h], D. Xiao[38,k,l], G.Y. Xiao[42], S.Y. Xiao[1], Y.L. Xiao[12,g], Z.J. Xiao[41], C. Xie[42], X.H. Xie[46,h], Y. Xie[50], Y.G. Xie[1,58], Y.H. Xie[6], Z.P. Xie[71,58], T.Y. Xing[1,63], C.F. Xu[1,63], C.J. Xu[59], G.F. Xu[1], H.Y. Xu[66], M. Xu[71,58], Q.J. Xu[16], Q.N. Xu[30], W. Xu[1], W.L. Xu[66], X.P. Xu[55], Y.C. Xu[77], Z.P. Xu[42], Z.S. Xu[63], F. Yan[12,g], L. Yan[12,g], W.B. Yan[71,58], W.C. Yan[80], X.Q. Yan[1], H.J. Yang[51,f], H.L. Yang[34], H.X. Yang[1], Tao Yang[1], Y. Yang[12,g], Y.F. Yang[43], Y.X. Yang[1,63], Yifan Yang[1,63], Z.W. Yang[38,k,l], Z.P. Yao[50], M. Ye[1,58], M.H. Ye[8], J.H. Yin[1], Z.Y. You[59], B.X. Yu[1,58,63], C.X. Yu[43], G. Yu[1,63], J.S. Yu[25,i], T. Yu[72], X.D. Yu[46,h], Y.C. Yu[80], C.Z. Yuan[1,63], J. Yuan[34], L. Yuan[2], S.C. Yuan[1], Y. Yuan[1,63], Y.J. Yuan[45], Z.Y. Yuan[59], C.X. Yue[39], A.A. Zafar[73], F.R. Zeng[50], S.H. Zeng[72], X. Zeng[12,g], Y. Zeng[25,i], Y.J. Zeng[59], X.Y. Zhai[34], Y.C. Zhai[50], Y.H. Zhan[59], A.Q. Zhang[1,63], B.L. Zhang[1,63], B.X. Zhang[1], D.H. Zhang[43], G.Y. Zhang[19], H. Zhang[80], H. Zhang[71,58], H.C. Zhang[1,58,63], H.H. Zhang[34], H.H. Zhang[59], H.Q. Zhang[1,58,63], H.R. Zhang[71,58], H.Y. Zhang[1,58], J. Zhang[80], J. Zhang[59], J.J. Zhang[52], J.L. Zhang[20], J.Q. Zhang[41], J.S. Zhang[12,g], J.W. Zhang[1,58,63], J.X. Zhang[38,k,l], J.Y. Zhang[1], J.Z. Zhang[1,63], Jianyu Zhang[63], L.M. Zhang[61], Lei Zhang[42], P. Zhang[1,63], Q.Y. Zhang[34], R.Y. Zhang[38,k,l], Shuihan Zhang[1,63], Shulei Zhang[25,i], X.D. Zhang[45], X.M. Zhang[1], X.Y. Zhang[50], Y. Zhang[72], Y.T. Zhang[80], Y.H. Zhang[1,58], Y.M. Zhang[39],

JHEP05(2024)335

Yan Zhang[71,58], Yao Zhang[1], Z.D. Zhang[1], Z.H. Zhang[1], Z.L. Zhang[34], Z.Y. Zhang[76], Z.Y. Zhang[43], Z.Z. Zhang[45], G. Zhao[1], J.Y. Zhao[1,63], J.Z. Zhao[1,58], Lei Zhao[71,58], Ling Zhao[1], M.G. Zhao[43], N. Zhao[78], R.P. Zhao[63], S.J. Zhao[80], Y.B. Zhao[1,58], Y.X. Zhao[31,63], Z.G. Zhao[71,58], A. Zhemchugov[36,b], B. Zheng[72], B.M. Zheng[34], J.P. Zheng[1,58], W.J. Zheng[1,63], Y.H. Zheng[63], B. Zhong[41], X. Zhong[59], H. Zhou[50], J.Y. Zhou[34], L.P. Zhou[1,63], S. Zhou[6], X. Zhou[76], X.K. Zhou[6], X.R. Zhou[71,58], X.Y. Zhou[39], Y.Z. Zhou[12,g], J. Zhu[43], K. Zhu[1], K.J. Zhu[1,58,63], K.S. Zhu[12,g], L. Zhu[34], L.X. Zhu[63], S.H. Zhu[70], S.Q. Zhu[42], T.J. Zhu[12,g], W.D. Zhu[41], Y.C. Zhu[71,58], Z.A. Zhu[1,63], J.H. Zou[1], J. Zu[71,58]

[1] *Institute of High Energy Physics, Beijing 100049, People's Republic of China*
[2] *Beihang University, Beijing 100191, People's Republic of China*
[3] *Bochum Ruhr-University, D-44780 Bochum, Germany*
[4] *Budker Institute of Nuclear Physics SB RAS (BINP), Novosibirsk 630090, Russia*
[5] *Carnegie Mellon University, Pittsburgh, Pennsylvania 15213, USA*
[6] *Central China Normal University, Wuhan 430079, People's Republic of China*
[7] *Central South University, Changsha 410083, People's Republic of China*
[8] *China Center of Advanced Science and Technology, Beijing 100190, People's Republic of China*
[9] *China University of Geosciences, Wuhan 430074, People's Republic of China*
[10] *Chung-Ang University, Seoul, 06974, Republic of Korea*
[11] *COMSATS University Islamabad, Lahore Campus, Defence Road, Off Raiwind Road, 54000 Lahore, Pakistan*
[12] *Fudan University, Shanghai 200433, People's Republic of China*
[13] *GSI Helmholtzcentre for Heavy Ion Research GmbH, D-64291 Darmstadt, Germany*
[14] *Guangxi Normal University, Guilin 541004, People's Republic of China*
[15] *Guangxi University, Nanning 530004, People's Republic of China*
[16] *Hangzhou Normal University, Hangzhou 310036, People's Republic of China*
[17] *Hebei University, Baoding 071002, People's Republic of China*
[18] *Helmholtz Institute Mainz, Staudinger Weg 18, D-55099 Mainz, Germany*
[19] *Henan Normal University, Xinxiang 453007, People's Republic of China*
[20] *Henan University, Kaifeng 475004, People's Republic of China*
[21] *Henan University of Science and Technology, Luoyang 471003, People's Republic of China*
[22] *Henan University of Technology, Zhengzhou 450001, People's Republic of China*
[23] *Huangshan College, Huangshan 245000, People's Republic of China*
[24] *Hunan Normal University, Changsha 410081, People's Republic of China*
[25] *Hunan University, Changsha 410082, People's Republic of China*
[26] *Indian Institute of Technology Madras, Chennai 600036, India*
[27] *Indiana University, Bloomington, Indiana 47405, USA*
[28] *INFN Laboratori Nazionali di Frascati , (A)INFN Laboratori Nazionali di Frascati, I-00044, Frascati, Italy; (B)INFN Sezione di Perugia, I-06100, Perugia, Italy; (C)University of Perugia, I-06100, Perugia, Italy*
[29] *INFN Sezione di Ferrara, (A)INFN Sezione di Ferrara, I-44122, Ferrara, Italy; (B)University of Ferrara, I-44122, Ferrara, Italy*
[30] *Inner Mongolia University, Hohhot 010021, People's Republic of China*
[31] *Institute of Modern Physics, Lanzhou 730000, People's Republic of China*
[32] *Institute of Physics and Technology, Peace Avenue 54B, Ulaanbaatar 13330, Mongolia*
[33] *Instituto de Alta Investigación, Universidad de Tarapacá, Casilla 7D, Arica 1000000, Chile*
[34] *Jilin University, Changchun 130012, People's Republic of China*
[35] *Johannes Gutenberg University of Mainz, Johann-Joachim-Becher-Weg 45, D-55099 Mainz, Germany*
[36] *Joint Institute for Nuclear Research, 141980 Dubna, Moscow region, Russia*
[37] *Justus-Liebig-Universitaet Giessen, II. Physikalisches Institut, Heinrich-Buff-Ring 16, D-35392 Giessen, Germany*
[38] *Lanzhou University, Lanzhou 730000, People's Republic of China*

[39] *Liaoning Normal University, Dalian 116029, People's Republic of China*
[40] *Liaoning University, Shenyang 110036, People's Republic of China*
[41] *Nanjing Normal University, Nanjing 210023, People's Republic of China*
[42] *Nanjing University, Nanjing 210093, People's Republic of China*
[43] *Nankai University, Tianjin 300071, People's Republic of China*
[44] *National Centre for Nuclear Research, Warsaw 02-093, Poland*
[45] *North China Electric Power University, Beijing 102206, People's Republic of China*
[46] *Peking University, Beijing 100871, People's Republic of China*
[47] *Qufu Normal University, Qufu 273165, People's Republic of China*
[48] *Renmin University of China, Beijing 100872, People's Republic of China*
[49] *Shandong Normal University, Jinan 250014, People's Republic of China*
[50] *Shandong University, Jinan 250100, People's Republic of China*
[51] *Shanghai Jiao Tong University, Shanghai 200240, People's Republic of China*
[52] *Shanxi Normal University, Linfen 041004, People's Republic of China*
[53] *Shanxi University, Taiyuan 030006, People's Republic of China*
[54] *Sichuan University, Chengdu 610064, People's Republic of China*
[55] *Soochow University, Suzhou 215006, People's Republic of China*
[56] *South China Normal University, Guangzhou 510006, People's Republic of China*
[57] *Southeast University, Nanjing 211100, People's Republic of China*
[58] *State Key Laboratory of Particle Detection and Electronics, Beijing 100049, Hefei 230026, People's Republic of China*
[59] *Sun Yat-Sen University, Guangzhou 510275, People's Republic of China*
[60] *Suranaree University of Technology, University Avenue 111, Nakhon Ratchasima 30000, Thailand*
[61] *Tsinghua University, Beijing 100084, People's Republic of China*
[62] *Turkish Accelerator Center Particle Factory Group, (A)Istinye University, 34010, Istanbul, Turkey; (B)Near East University, Nicosia, North Cyprus, 99138, Mersin 10, Turkey*
[63] *University of Chinese Academy of Sciences, Beijing 100049, People's Republic of China*
[64] *University of Groningen, NL-9747 AA Groningen, The Netherlands*
[65] *University of Hawaii, Honolulu, Hawaii 96822, USA*
[66] *University of Jinan, Jinan 250022, People's Republic of China*
[67] *University of Manchester, Oxford Road, Manchester, M13 9PL, United Kingdom*
[68] *University of Muenster, Wilhelm-Klemm-Strasse 9, 48149 Muenster, Germany*
[69] *University of Oxford, Keble Road, Oxford OX13RH, United Kingdom*
[70] *University of Science and Technology Liaoning, Anshan 114051, People's Republic of China*
[71] *University of Science and Technology of China, Hefei 230026, People's Republic of China*
[72] *University of South China, Hengyang 421001, People's Republic of China*
[73] *University of the Punjab, Lahore-54590, Pakistan*
[74] *University of Turin and INFN, (A)University of Turin, I-10125, Turin, Italy; (B)University of Eastern Piedmont, I-15121, Alessandria, Italy; (C)INFN, I-10125, Turin, Italy*
[75] *Uppsala University, Box 516, SE-75120 Uppsala, Sweden*
[76] *Wuhan University, Wuhan 430072, People's Republic of China*
[77] *Yantai University, Yantai 264005, People's Republic of China*
[78] *Yunnan University, Kunming 650500, People's Republic of China*
[79] *Zhejiang University, Hangzhou 310027, People's Republic of China*
[80] *Zhengzhou University, Zhengzhou 450001, People's Republic of China*

[a] *Deceased*
[b] *Also at the Moscow Institute of Physics and Technology, Moscow 141700, Russia*
[c] *Also at the Novosibirsk State University, Novosibirsk, 630090, Russia*
[d] *Also at the NRC "Kurchatov Institute", PNPI, 188300, Gatchina, Russia*
[e] *Also at Goethe University Frankfurt, 60323 Frankfurt am Main, Germany*
[f] *Also at Key Laboratory for Particle Physics, Astrophysics and Cosmology, Ministry of Education; Shanghai Key Laboratory for Particle Physics and Cosmology; Institute of Nuclear and Particle Physics, Shanghai 200240, People's Republic of China*

JHEP05(2024)335

[g] Also at Key Laboratory of Nuclear Physics and Ion-beam Application (MOE) and Institute of Modern Physics, Fudan University, Shanghai 200443, People's Republic of China
[h] Also at State Key Laboratory of Nuclear Physics and Technology, Peking University, Beijing 100871, People's Republic of China
[i] Also at School of Physics and Electronics, Hunan University, Changsha 410082, China
[j] Also at Guangdong Provincial Key Laboratory of Nuclear Science, Institute of Quantum Matter, South China Normal University, Guangzhou 510006, China
[k] Also at MOE Frontiers Science Center for Rare Isotopes, Lanzhou University, Lanzhou 730000, People's Republic of China
[l] Also at Lanzhou Center for Theoretical Physics, Lanzhou University, Lanzhou 730000, People's Republic of China
[m] Also at the Department of Mathematical Sciences, IBA, Karachi 75270, Pakistan
[n] Also at Ecole Polytechnique Federale de Lausanne (EPFL), CH-1015 Lausanne, Switzerland
[o] Also at Helmholtz Institute Mainz, Staudinger Weg 18, D-55099 Mainz, Germany

JHEP05(2024)335